MOLECULAR SIMULATION STUDY ON THE INTERACTION OF NANOPARTICLES WITH CLAY MINERALS: C_{60} ON SURFACES OF PYROPHYLLITE AND KAOLINITE

Huijun Zhou[1,2], Meng Chen[1], Lifang Zhu[3], Lin Li[1,2], Runliang Zhu[1,*], and Hongping He[1,2]

[1] CAS Key Laboratory of Mineralogy and Metallogeny/Guangdong Provincial Key Laboratory of Mineral Physics and Materials, Guangzhou Institute of Geochemistry, Chinese Academy of Sciences (CAS), Guangzhou 510640, China
[2] University of Chinese Academy of Sciences, Beijing 100049, China
[3] Zhejiang University of Water Resources and Electric Power, Hangzhou 310018, China

Abstract—Buckminsterfullerene (C_{60}) is one of the most important carbon-based nanoparticles (CNPs). Industrial-scale production of C_{60} has reached the level of tons; release to the environment has been confirmed (Tremblay, 2002; Qiao *et al*., 2007). The present study was devoted to study of the effect of clay minerals on the migration process of C_{60}. Molecular dynamics (MD) simulations were used to study the interaction of CNP_S with clay minerals through study of the adsorption of C_{60} on various surfaces of kaolinite and pyrophyllite in vacuum and aqueous environments. Two kinds of surfaces, hydrophobic siloxane surfaces and hydrophilic hydroxyl surfaces, were investigated. C_{60} is mainly adsorbed onto the vacancy of the six-membered ring, composed of SiO_4 tetrahedra or AlO_6 octahedra, on clay-mineral surfaces. A single adsorption layer consisting of C_{60} molecules with an ordered hexagonal arrangement is presented for all surfaces in vacuum. In aqueous environments, however, the monolayer appears on the siloxane surfaces only, while a cluster of C_{60} molecules is formed on the hydroxyl surfaces. Free energies prove that the attachment of two C_{60} molecules is stronger than the adsorption of C_{60} onto the hydroxyl surface in water, which is the reason for unfavorable formation of C_{60} monolayer. On the other hand, the adsorption free energy is more negative on the hydrophobic siloxane surface, explaining the monolayer formation. The existence of water, which forms hydration layers on the surfaces of clay minerals, produces energy barriers, and reduces the adsorption affinity to some extent. Because clay minerals act as geosorbents in the environment, the present study is significant in terms of understanding the migration and fate of CNP_S in nature.

Key Words—Adsorption, C_{60}, Free Energy, Kaolinite, MD Simulation, Pyrophyllite.

INTRODUCTION

Carbon-based nanomaterials are used in a wide variety of fields such as environmental remediation, electrochemistry, the chemical industry, and medicine because of their unique physical and chemical properties (Gogotsi, 2006; Mauter and Elimelech, 2008; Pumera, 2010; Scida *et al*., 2011; Cha *et al*., 2013; Kouijzer *et al*., 2014; Ahmadi *et al*., 2017). Buckminsterfullerene (C_{60}) is one of the most important CNP_S and has been used widely in the synthesis of other materials (Guldi *et al*., 2002; Goyal *et al*., 2005; Han *et al*., 2015). Industrial-scale production of C_{60} has reached the level of tons (Zhu *et al*., 2013; Dellinger *et al*., 2015). As a result, a large amount of CNPs has been discharged into the environment and is considered to be biologically toxic (Sayes *et al*., 2004; Liu *et al*., 2010; Hou *et al*., 2011; Song *et al*., 2012). Under ambient conditions in water, fullerenes can generate superoxide anions; these oxygen radicals were deemed by Sayes *et al.* (2004) to be responsible for membrane damage and cell death. Fullerene-inducing oxidative damage in human embryo-nic liver cells was proved by Zhang *et al.* (2011). The potential threats of C_{60} to the environment and human health are of significant concern. In aqueous environments C_{60} may aggregate and interact with various natural geosorbents and this plays a key role in their migration and enrichment in the environment (Bergaya *et al*., 2006; Chen and Jafvert, 2009; Li *et al*., 2009; Fortner *et al*., 2012). Nano-scale aggregates are formed readily from C_{60} in water when its content exceeds 7.96 ng/L (Fortner *et al*., 2005; Jafvert and Kulkarni, 2008; Labille *et al*., 2009). As the size of individual C_{60} molecules is smaller than those of C_{60} aggregates, the individual molecule might easily be captured by natural micropores and mesopores and adsorbed by geosorbents. As the solubility of C_{60} is so limited and its size so small, detection by most instruments is impossible; the interaction behaviors between C_{60} molecules and natural geosorbents have not yet been explored thoroughly.

Molecular dynamics (MD) simulations have been used to study hydration and aggregation of C_{60} in water (Li *et al*., 2005; Choudhury, 2006; Kim and Bedrov, 2008; Chen and Jafvert, 2009; Maciel *et al*., 2009).

Through simulation, the microstructure of C_{60} in the aqueous phase and its thermodynamic behavior were elucidated (Choudhury, 2006; Kim and Bedrov, 2008). Clay minerals generally appear in aqueous environments and they are natural geosorbents. The adsorption of various chemicals on clay minerals has been investigated intensively using molecular simulations (Teppen et al., 1998; Yu et al., 2000a; Cygan et al., 2009; Heinz, 2012). Classic atomic force fields such as CLAYFF (Cygan et al., 2004; Zhu et al., 2011) and PFF (Heinz et al., 2005) for describing clay minerals have been used. Molecular dynamics simulations were used to examine the adsorption of U(VI) onto an external montmorillonite surface (Greathouse and Cygan, 2005). The adsorption of proteins on clay-mineral surfaces was studied by Yu et al. (2000b). Studies of the adsorption of C_{60} on clay minerals are still rare, however (Thundat et al., 1993; Zhu et al., 2013).

The purpose of the present study was to investigate the adsorption of C_{60} on various surfaces of clay minerals by carrying out MD simulations of C_{60} adsorbed on the surfaces of pyrophyllite and kaolinite. A further objective was to calculate the adsorption free energy and elucidate the microstructure of adsorption of one or several C_{60} molecules on clay-mineral surfaces. Understanding such 'micro-level' information is important in revealing the migration and fate of carbon nanomaterials in aqueous environments.

MD SIMULATION DETAILS

Depending on sheet stacking, clay minerals are divided into TO and TOT types (T represents the sheets of SiO_4 tetrahedra and O represents the sheets of AlO_6 octahedra). Tetrahedra of the T sheet are connected in six-member rings, as are octahedra in the O sheet (Figure 1). Two types of external surfaces, siloxane and hydroxyl, are presented, therefore (Bergaya et al., 2006). Two representative minerals, kaolinite (TO type), and pyrophyllite (TOT type) were selected for the present study. Kaolinite ($Al_4[Si_4O_{10}](OH)_8$) is composed of a T sheet and an O sheet (Figure 1a); two different surfaces, i.e. siloxane (Figure 1b) and hydroxyl (Figure 1c), are encountered in the [001] direction (Bailey, 1963; Bish, 1993; Bergaya et al., 2006). TO layers of kaolinite are stacked through hydrogen-bond connections (Bish, 1993). Pyrophyllite, $Al_2[Si_4O_{10}](OH)_2$, is composed of TOT layers arranged parallel to the ab plane (Figure 1d), which can be imagined as a hexagonally ordered O sheet sandwiched between two T siloxane sheets (Gruner, 1934; Hendricks, 1940; Grim, 1968; Lee and Guggenheim, 1981). The siloxane surface is the external surface of the T sheet in the [001] direction (Figure 1e). Adjacent TOT layers are stacked with van der Waals interactions.

The simulated kaolinite supercells consist of 72 unit cells ($6 \times 6 \times 2$ units in a, b, and c dimensions) with C1
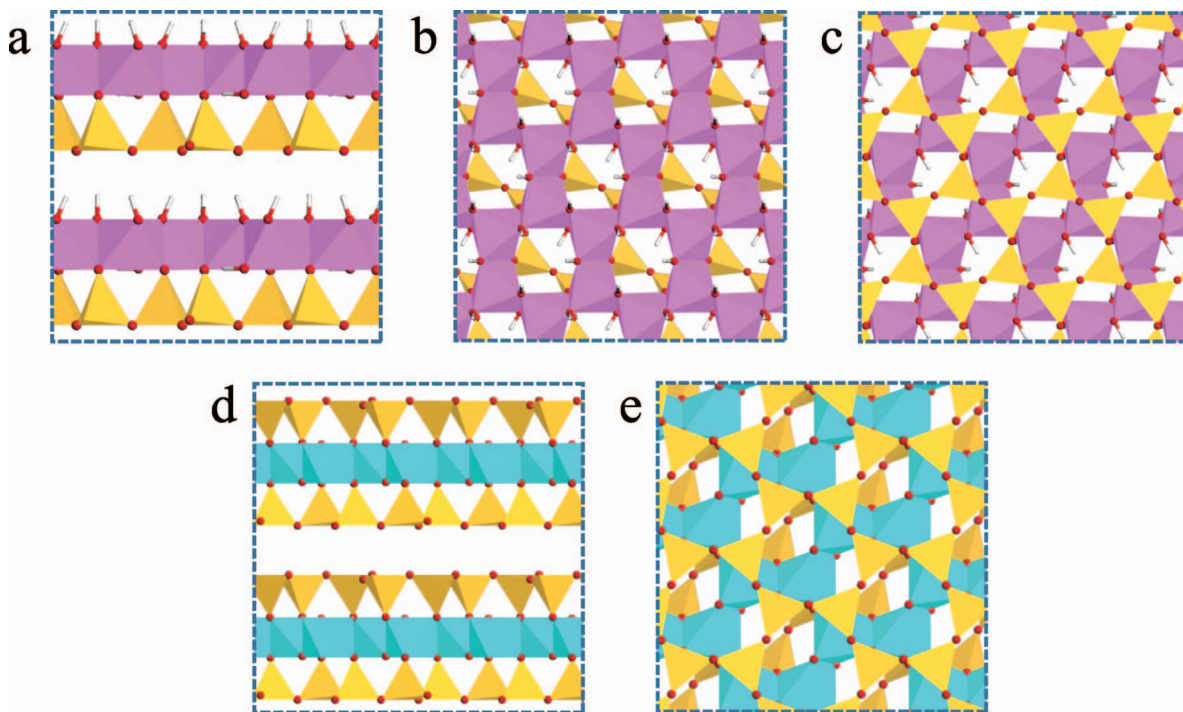

Figure 1. Different views of the crystal structures investigated: (a) layers of kaolinite; (b) hydroxyl surface of kaolinite; (c) siloxane surface of kaolinite; (d) layers of pyrophyllite; and (e) siloxane surface of pyrophyllite. The layers are parallel to the ab plane and surfaces along the [001] direction.

symmetry (Bish, 1993). The supercell is ~3.092 and 5.365 nm long in x and y axes, respectively. An inverted supercell was stacked on top of another, with two vacuum slabs (8.7 nm) inserted between them through periodic boundary conditions (Figure 2a). The total height of the model is 20.0 nm. Thus, two kinds of surfaces, siloxane and hydroxyl, were built. The two kaolinite slabs were inverted with respect to each other to ensure that the periodic simulation cell has no net dipole (Warne *et al.*, 2000). This system has a total of 4896 atoms. The pyrophyllite supercells simulated, with a total of 5120 atoms, consist of 128 unit cells ($8 \times 8 \times 2$ units in a, b, and c dimensions) with $C1$ symmetry (Lee and Guggenheim, 1981). The supercell is ~4.128 and 7.172 nm long in the x and y axes, respectively. A vacuum slab with a thickness of ~8.4 nm was added on the top of the slab along the z axes (Figure 2b). These models were used to study the adsorption of one or several C_{60} molecules in vacuum on various surfaces, *i.e.* the siloxane surface of pyrophyllite (P-SiO), and the siloxane and hydroxyl surfaces of kaolinite (K-SiO and K-OH). After equilibrium of adsorption simulation in vacuum, water with a density of ~1 g/cm^3 was added into the vacuum slabs to study the adsorption of C_{60} in aqueous phases on various surfaces.

The *GROMACS* 5.1.2 program (Hess *et al.*, 2008) was used to perform simulations at a temperature of 298 K. All models in these simulations were in three-dimensional periodic boundary conditions (Makov and Payne, 1995). The equations of motion were integrated with the leapfrog

algorithm and with a time step of 1.0 fs. The electrostatic interaction was evaluated using the particle-mesh Ewald (PME) method. For all simulations of the pyrophyllite system, the short cut-off radius was set to 1.95 nm, and for the kaolinite system, to 1.50 nm, corresponding to approximately half of the shortest dimension of the respective boxes. The *CLAYFF* force field (Cygan *et al.*, 2004) was used to describe pyrophyllite and kaolinite, while the flexible SPC model was for water (Robinson *et al.*, 1996). The *CVFF* (Dauber-Osguthorpe *et al.*, 1998), *Dreiding* (Mayo *et al.*, 1990), *Amber* (Cornell *et al.*, 1995), and *GMX* (Qiao *et al.*, 2007) force fields have been used to describe C_{60}. The parameters of *OPLS-AA* (Jorgensen *et al.*, 1996) force fields were used in the present study because they describe well C_{60} in solvent (Monticelli, 2012).

In each MD simulation, an energy minimization was carried out to relax the system at first. For systems with vacuum slabs, simulations were performed in canonical ensemble (NVT) for 10 ns. Data were saved for analysis every 0.1 ps in the last 5 ns of simulations. The Nosé-Hoover thermostat (Evans and Holian, 1985) was used to control the temperature. On the other hand, for systems with aqueous slabs, after energy minimization, isothermal-isobaric (NPT) MD simulations were employed at 298 K and 1.0 atm for 10 ns, with the Nosé-Hoover thermostat and Parrinello-Rahman barostat (Parrinello and Rahman, 1981; Nosé and Klein, 1983). In the present study, the pressure was imposed only in the normal z direction. As a result, only the box shape in the
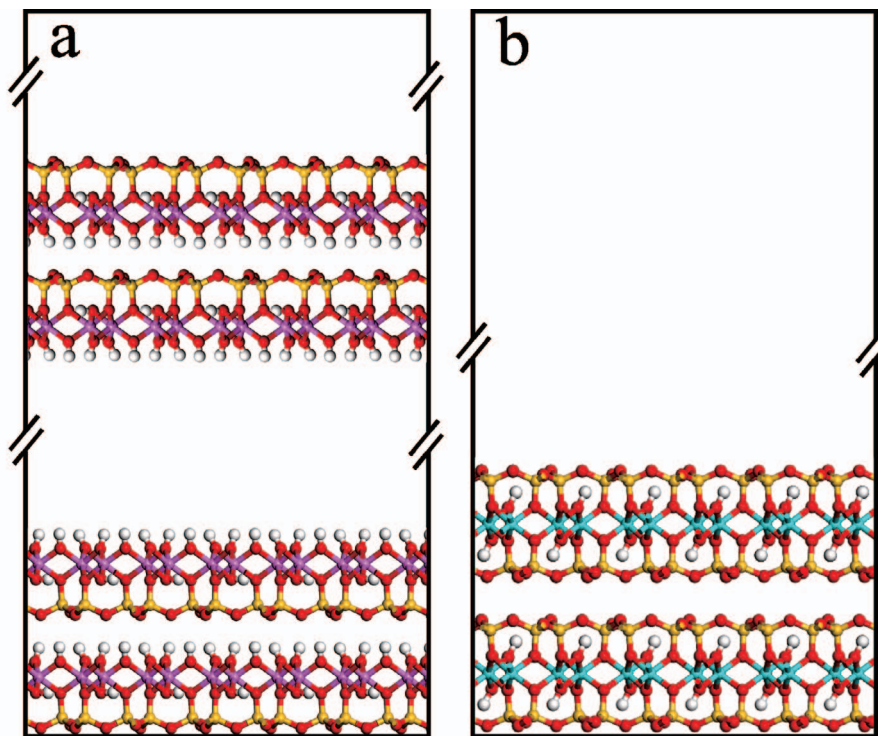

Figure 2. Sketches of simulation systems: (a) kaolinite/vacuum; (b) pyrophyllite/vacuum.

z direction was fluctuated. Subsequent runs were performed in NVT ensemble for 10 ns. Data were saved for analysis every 0.1 ps in the last 5 ns simulations.

The free energy of adsorption (potential of mean force, PMF) is a physical quantity which shows whether the process of C_{60} adsorption is spontaneous (Adamson and Gast, 1967; Liu, 2009). In the present study, the free energy of adsorption of C_{60} in vacuum or in aqueous phases on various surfaces (P-SiO, K-SiO and K-OH surfaces) was derived through calculation of the PMF along the desorption trajectory. For the K-OH surface, the average position of Al atoms of the outermost octahedral sheet was used to characterize the surface position, while for the P-SiO and K-SiO surfaces, the average position of Si atoms of the outermost tetrahedral sheet was used. Firstly, the config- uration at the end of the NVT simulation was used to perform another 2 ns NVT simulation by constraining the center of mass of a C_{60} with regard to the *z* axes (Ryckaert *et al.*, 1977; Hess *et al.*, 1997). Then, the C_{60} was moved away from the surface by ~0.01 nm (Figure 3), and a new 2 ns constrained MD simulation also in NVT ensemble was performed. This process was repeated several times until the distance between C_{60} and surface reached ~1.50 nm. Subsequently, the C_{60} was moved away with a 0.05 nm increment and 2 ns constrained MD simulations were performed for each new configuration. In the end, the C_{60} was ~2.50 nm from the surface in vacuum and ~3.00 nm away in water. The PMF was obtained by integrating the mean force required to constrain the molecule along the move trajectory.

RESULTS AND DISCUSSION

The adsorption of a single C_{60} molecule on surfaces

Adsorption sites. The centroid positions of C_{60} and atoms of clay surfaces in each frame were counted to show the adsorption sites of C_{60} (Figure 4). C_{60} was adsorbed favorably onto the vacancy of the six- membered ring, made either of SiO_4 tetrahedra or AlO_6 octahedra, irrespective of the environment, which implies that the strong van der Waals interaction between C_{60} and six-membered rings on surfaces leads to the adsorption. The adsorption of ions on clay surfaces was studied by Vasconcelos *et al.* (2007) who discovered that ions adsorbed preferentially into the vacancies of six-membered rings. That study indicated that the six-membered rings of clay surfaces are active sites of adsorption. The trajectories of C_{60} are obviously more dispersed at the vacuum−clay interfaces, implying a greater degree of freedom. In the aqueous phase, C_{60} is restricted to locations in nearby six-membered rings. The hydration of C_{60} retards its movement. To show the hydration structure clearly, density profiles of C_{60} and water were derived, and are shown below.

Atomic Z density. In vacuum, C_{60} locates at distances of 0.34−1.14 nm, 0.27−1.10 nm, and 0.27−1.06 nm above the K-OH, K-SiO, and P-SiO surfaces, respectively (Figure 5a,b,c). The locations of two siloxane surfaces are almost identical, which shows that the adsorption of C_{60} is, in general, on the siloxane surfaces of clay minerals through van der Waals interactions of similar magnitudes independent of surface chemistry.
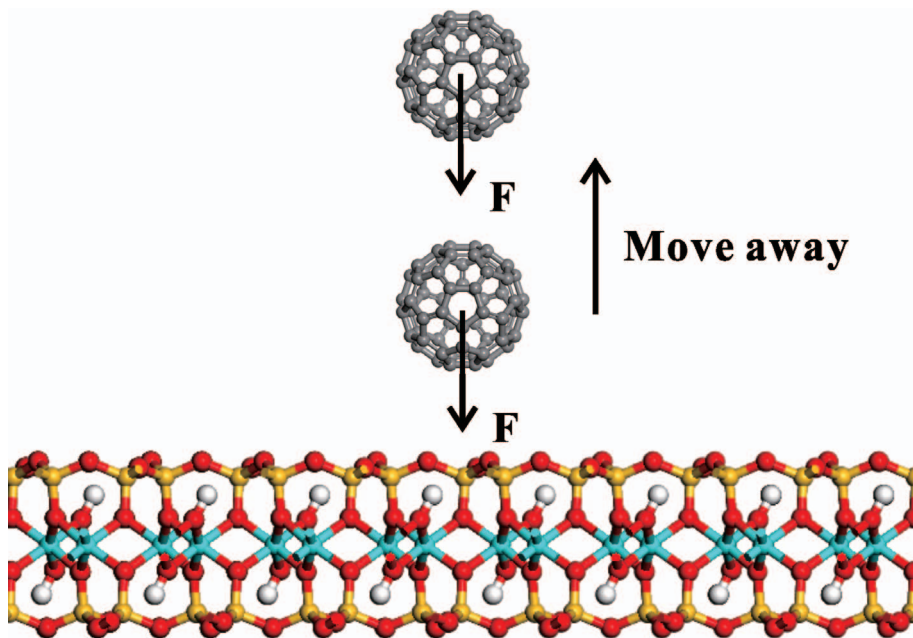

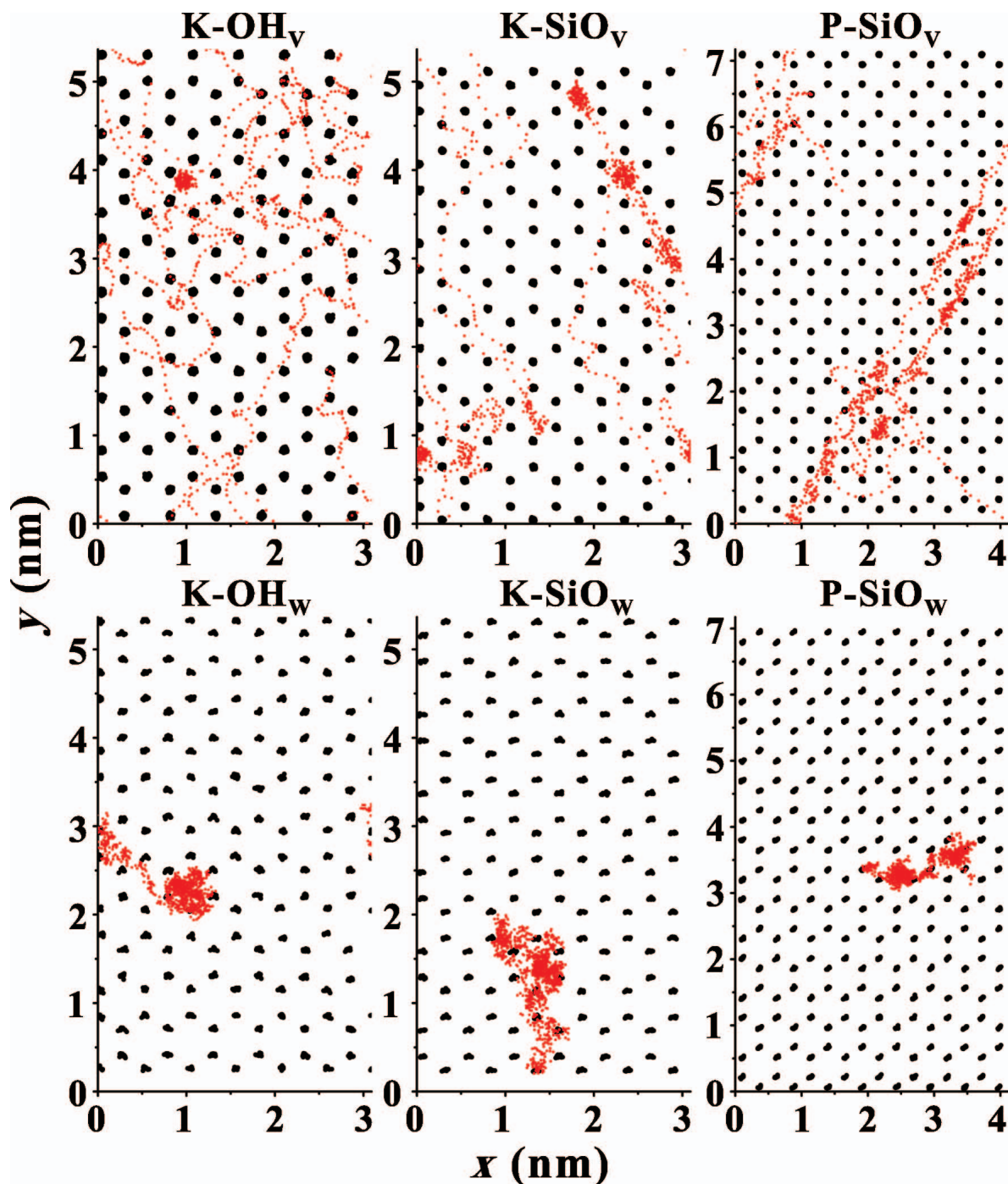Figure 3. Calculation process of adsorption free energy

Figure 4. The adsorption sites of 1 C_{60}. The black spots (larger) represent the centroid position of reference atoms (Al for hydroxyl surface and Si for siloxane surface). The red spots (smaller) represent the centroid position of C_{60}. K-OH: hydroxyl surface of kaolinite; K-SiO: siloxane surface of kaolinite; P-SiO: siloxane surface of pyrophyllite; the upper panels represent the vacuum environment (v) and the lower panels, the aqueous environment (w).

In the aqueous phase, C_{60} locates at distances of 0.25−1.11 nm and 0.26−1.10 nm above K-SiO and P-SiO surfaces, respectively (Figure 5e,f), similar to the situations in vacuum. The van der Waals interactions between C_{60} and surfaces play a determinant role on adsorption behaviors. C_{60} locates at distances of 0.59−1.45 nm above the K-OH surface (Figure 5d), however, which is greater than the distance in vacuum (0.34−1.14 nm). Furthermore, water molecules form several hydration layers on clay surfaces, located at
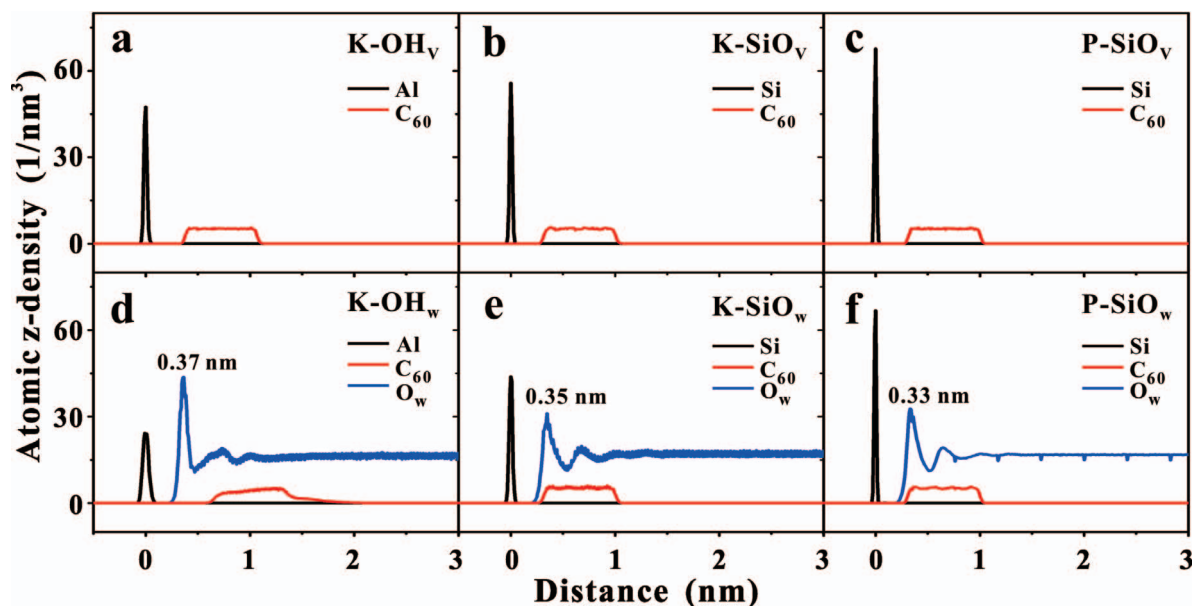
Figure 5. Atomic density profiles on each surface. To aid clarity, the densities of Al and Si have been scaled by 0.2, while that of O_w has been multiplied by 0.5 and that of C_{60} on pyrophyllite siloxane surface has been multiplied by 1.78 (the ratio between the *ab*-plane areas of the pyrophyllite and the kaolinite slabs) for better observation. Al: Al atoms of the hydroxyl surface; Si: Si atoms of the siloxane surfaces; O_w: O atoms of H_2O. K-OH, K-SiO, and P-SiO are the same as in Figure 4; the upper panels (a,b,c) represent the vacuum environment (v) and the lower panels (d,e,f) represent the aqueous environment (w).

0.18−1.10 nm, 0.16−0.84 nm, and 0.14−0.82 nm, respectively (Figure 5d,e,f). Above the K-SiO and P-SiO surfaces, the locations of C_{60} show that C_{60} has broken through the first hydration layer (0.35 nm and 0.33 nm), while the location of fullerene (0.59−1.45 nm) shows that the fullerene has not broken through the first hydration layer (0.37 nm) above the K-OH surface (Figure 5d,e,f). This implies that the interaction between C_{60} and siloxane surfaces is of similar magnitude to that between water molecules and siloxane surfaces, whereas the interaction between C_{60} and the hydroxyl surface is weaker than that between water molecules and hydroxyl surfaces.

The hydroxyl surface is known to be hydrophilic because it forms hydrogen bonds with water molecules (López-Lilao *et al.*, 2017). This leads to a much greater adsorption density of water as shown by the sharp density peak corresponding to the first hydration layer (Figure 5d). The siloxane surfaces are generally thought to be hydrophobic and interactions between them and water are also due to van der Waals forces. In general, the hydrogen-bond interaction is stronger than the van der Waals interaction, which may be why C_{60} cannot break through the hydration layer on the hydroxyl surface.

Adsorption free energy. The mean force and PMF are calculated to determine the strength of C_{60} adsorbed on clay-mineral surfaces. The positive value of mean force represents repulsion between the surface and C_{60}, while the negative value represents attraction (Figure 6). In vacuum, with the decrease in distance between the clay-mineral surface and C_{60}, the force between them changes from zero to attraction until the distance is <0.66 nm (position in Figure 6) above the K-SiO and P-SiO surfaces, and 0.72 nm (position in Figure 6) above the K-OH surface. When the distance decreases, it changes from attraction to repulsion. In aqueous environments, the force changes from attraction to repulsion also at a distance of 0.66 nm (position in Figure 6) above the K-SiO and P-SiO surface, but at 1.01 nm (position in Figure 6) above the K-OH surface. On the other hand, at greater distances above surfaces, the force becomes fluctuated, revealing the influence of hydration layers. The PMF is derived based on the variation of force along the reaction coordinate; the free energy of adsorption is achieved. Positions ①, ②, ③, and ④, correspond to PMF minima.

The free energy of C_{60} adsorbed from vacuum onto the siloxane surface (−0.530 eV) is more negative than that onto the hydroxyl surface (−0.391 eV). On the other hand, adsorption on the siloxane surfaces of kaolinite and pyrophyllite is almost indistinguishable. This implies that the surface chemistry determines the adsorption free energy. Adsorption onto the hydrophobic siloxane surface is more favored even in vacuum. In the aqueous phase, the adsorption free energy is less negative on all of the surfaces examined, which implies that the hydration of clay surfaces and C_{60} retards C_{60} adsorption to some extent. The force oscillation caused by the hydration layers is also reflected in the fluctuation of PMF in aqueous phase. Once again, the adsorption
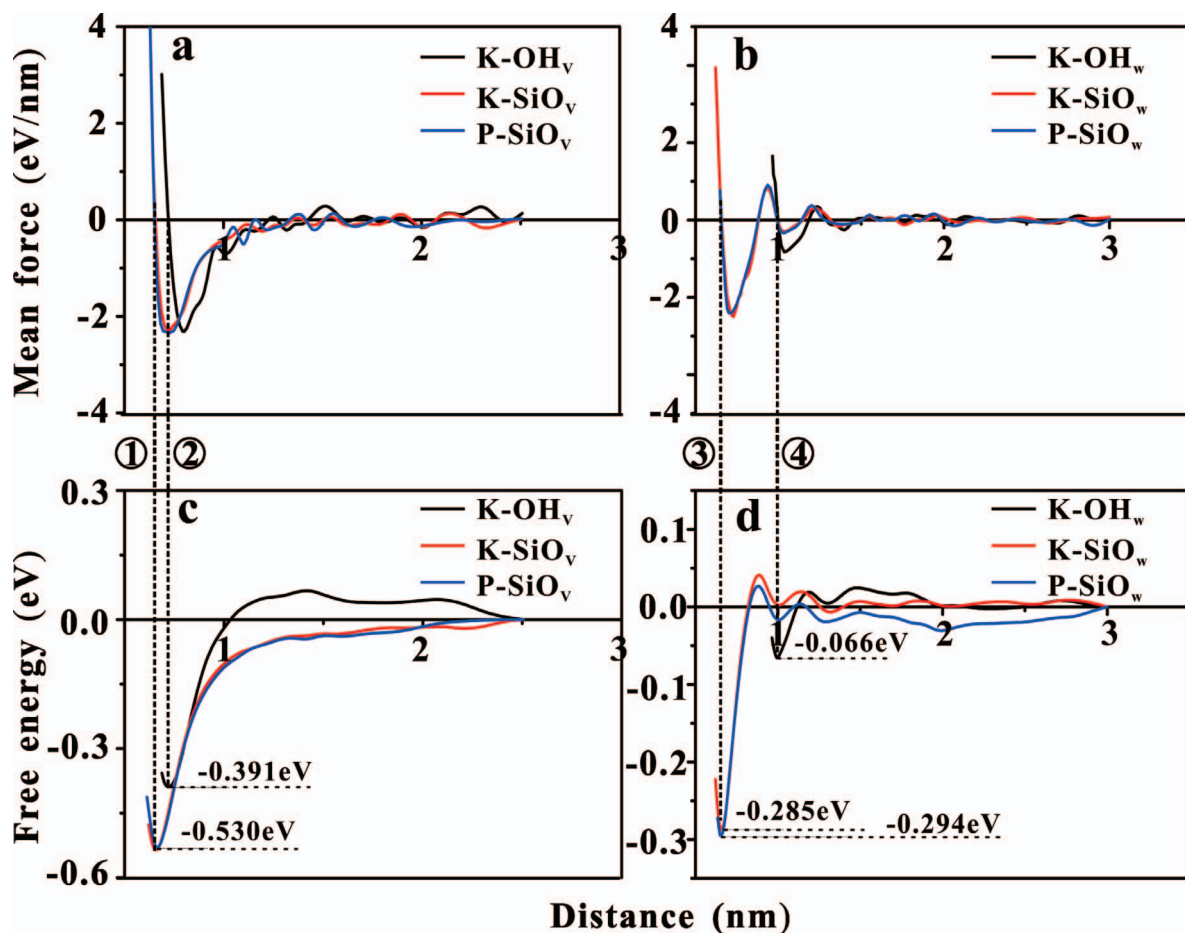
Figure 6. The mean force of C_{60} along the move trajectory and the free energy. The free energy at the end of the move trajectory is set to 0. K-OH, K-SiO, and P-SiO are the same as in Figure 4; the left panels (a,c) represent the vacuum environment (v) and the right panels (b,d) represent the aqueous environment (w).

free energies are similar on K-SiO (-0.285 eV) and P-SiO surfaces (-0.294 eV). Significantly, the free energy is obviously less negative on the K-OH surface (-0.066 eV). Because C_{60} cannot break through the first hydration layer on the K-OH surface in water (Figure 5d), the van der Waals interaction between it and the K-OH surface is weaker. Adsorption on the K-OH surface is, therefore, much weaker than on other surfaces. The hydrophobicity of a surface determines the adsorption behavior of C_{60}. In addition, the positions with the lowest free energies correspond to where C_{60} is adsorbed as shown in the density profiles (Figure 5).

The adsorption of multiple C_{60} molecules on surfaces

At the vacuum−clay interface, according to the snapshots (Figure 7), C_{60} molecules are adsorbed onto the vacancy of six-membered rings of clay surfaces, irrespective of surface type or C_{60} content. C_{60} molecules form a single adsorption layer on the clay surfaces. In the adsorption layer, C_{60} molecules are packed in orderly fashion into a hexagonal arrangement.

The distance between every two C_{60} molecules is almost the same, ~1.0 nm which suggests that the van der Waals interactions among C_{60} molecules and between C_{60} and clay surfaces both contributed to the adsorption of C_{60} molecules, leading to the aforementioned ordered arrangement.

In aqueous environments, C_{60} molecules are also arranged in orderly fashion as a single layer on the siloxane surface, and the adsorption sites are similar to those in vacuum. On the hydroxyl surface, however, C_{60} molecules tend to form a cluster rather than a single adsorption layer. This phenomenon can be attributed to the factor that the interaction between C_{60} and the hydroxyl surface in aqueous environment is much weaker, as disclosed by the less negative adsorption free energy (Figure 6d).

The z-direction density distribution confirms that C_{60} molecules form a single layer on the siloxane surfaces in water, as indicated by the phenomenon that the width of C_{60} distribution is almost constant when the amount of C_{60} is increased (Figure 8). The positions where C_{60} locate do not vary with the number of molecules
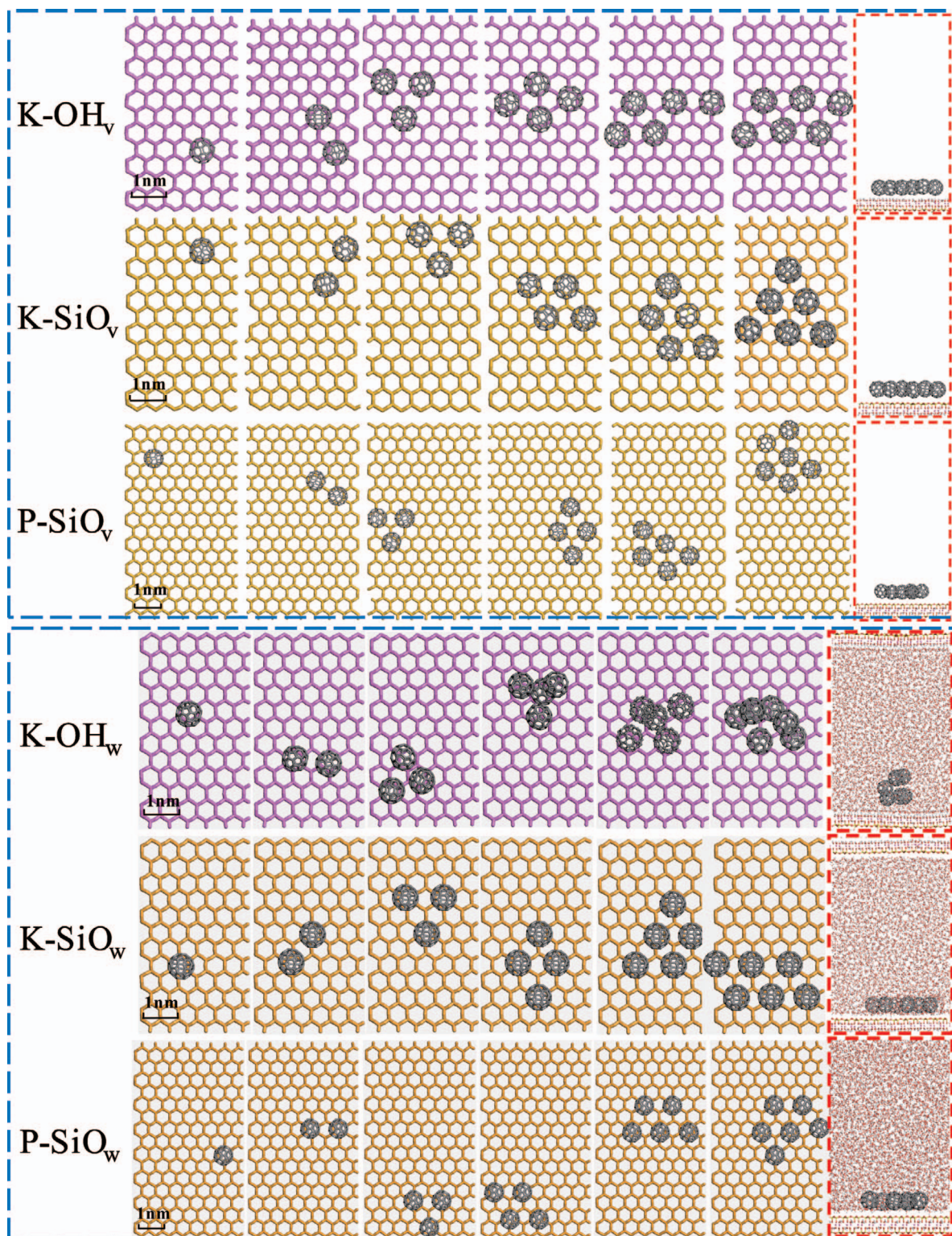
Figure 7. Snapshots of adsorption sites. Yellow six-membered rings represent silicon tetrahedra, pink six-membered rings represent aluminum octahedra. K-OH, K-SiO, P-SiO, and v, are the same as in Figure 4.
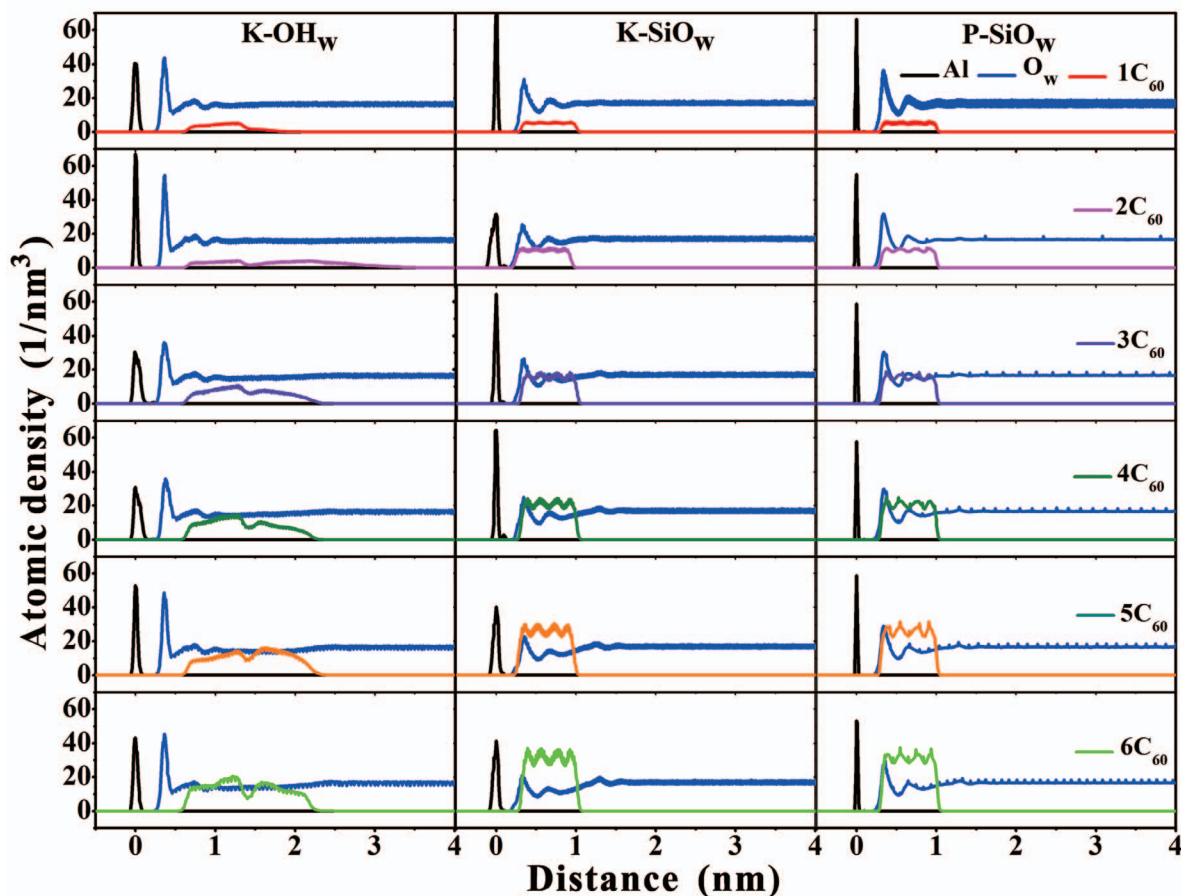
Figure 8. Atomic density profiles on each of the surfaces. For the purposes of clarity, densities of Al and Si have been scaled by 0.333, and that of C_{60} on the pyrophyllite siloxane surface have been multiplied by 1.78 (the ratio between the *ab*-plane areas of the pyrophyllite and the kaolinite slabs), while that of O_w atoms was multiplied by 0.5 to ease examination. K-OH, K-SiO, P-SiO, and w are the same as in Figure 4.

adsorbed. On the hydroxyl surface, however, the width of C_{60} distribution is much greater in the case of the adsorption of several molecules, which corresponds to cluster formation. The cluster adsorbed cannot break through the first hydration layer, consistent with the adsorption of a single molecule.

To show the arrangement among the C_{60} molecules adsorbed, radial distribution functions ($g(r)$) among C_{60} molecules were calculated (Figure 9). In all such situations, the peak $g(r)$ was located at ~1.0 nm, consistent with the distance between C_{60} molecules revealed in the snapshot (Figure 7). This distance is the same as that between two C_{60} molecules in water when the PMF between them achieves a minimum (Monticelli, 2012). Whether C_{60} molecules form an adsorption layer or a cluster, the interaction among them plays an important role in their aggregate structure, which favors a neighboring distance of ~1.0 nm. Monticelli (using the same force field) showed that the attachment free energy between two C_{60} molecules is ~−0.18 eV, which is obviously less negative than the adsorption free energy

on all the surfaces in vacuum and on siloxane surfaces in water. This is more negative than that on hydroxyl surfaces in water and explains why C_{60} molecules form a cluster on the hydroxyl surface in aqueous environments, but an adsorption layer in other cases.

CONCLUSIONS

In the present study MD simulations were used to study the adsorption of C_{60} molecules on various clay-mineral surfaces. The adsorption sites, adsorption configurations, and adsorption free energy values were established. According to the results obtained, C_{60} is adsorbed onto the vacancy of the six-membered ring on the clay-mineral surfaces both in vacuum and aqueous environment. C_{60} molecules exhibit a monolayer adsorption configuration with an ordered hexagonal arrangement on both the hydroxyl and siloxane surfaces in vacuum and siloxane surfaces in aqueous environments. On a hydroxyl surface in an aqueous environment, C_{60} molecules prefer to form clusters rather than a mono-
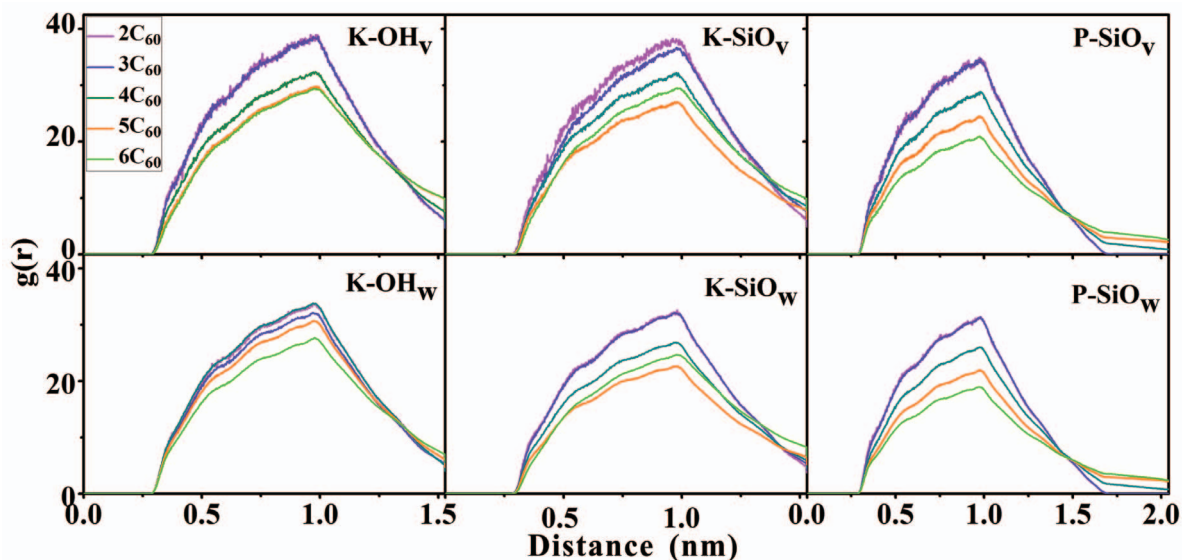
Figure 9. Radial distribution functions between C_{60} molecules. $2C_{60}-6C_{60}$ represents the amount of C_{60} in the system. K-OH, K-SiO, and P-SiO are the same as in Figure 4; the upper panels represent the vacuum environment (v) and the lower panels represent the aqueous environment (w).

layer. Adsorption free energy demonstrates that water molecules form energy barriers and reduce the adsorption affinity. The free energy for adsorption onto hydroxyl surface in water is less negative than that for the attachment of two C_{60} molecules. As a result, C_{60} molecules cannot break through the first hydration layer of the hydroxyl surface and form a cluster beyond the surface. On the other hand, siloxane surfaces, which many believe to be hydrophobic, exhibit a more negative adsorption free energy which favors monolayer adsorption. As such, clay minerals containing hydrophobic surfaces have a positive effect on C_{60} adsorption, which may be extended to other carbon-based nanoparticles. The calculation method in this paper can be extended to studying other adsorption behaviors on clay minerals. The present study sheds light on understanding the migration of carbon-based materials in aqueous environments where clay minerals exist as natural geosorbents.

REFERENCES

Adamson, A. W. and Gast, A.P. (1967) *Physical Chemistry of Surfaces*. Wiley, New Jersey, 400−408.

Ahmadi, M., Elmongy, H., Madrakian, T., and Abdel-Rehim, M. (2017) Nanomaterials as sorbents for sample preparation in bioanalysis: A review. *Analytica Chimica Acta*, **958**, 1−21.

Bailey, S.W. (1963) Polymorphism of kaolin minerals. *American Mineralogist*, **48**, 1196.

Bergaya, F., Theng, B.K.G., and Lagaly, G. (editors) (2006) *Handbook of Clay Science*. Elsevier, Amsterdam.

Bish, D.L. (1993) Rietveld refinement of the kaolinite structure at 1.5 K. *Clays and Clay Minerals*, **41**, 738−744.

Cha, C., Shin, S.R., Annabi, N., Dokmeci, M.R., and Khademhosseini, A. (2013) Carbon-based nanomaterials: multifunctional materials for biomedical engineering. *ACS Nano*, **7**, 2891−2897.

Chen, C.Y. and Jafvert, C.T. (2009) Sorption of buckminster-fullerene (C_{60}) to saturated soils. *Environmental Science & Technology*, **43**, 7370−7375.

Choudhury, N. (2006) A molecular dynamics simulation study of buckyballs in water: Atomistic versus coarse-grained models of c-60. *Journal of Chemical Physics*, **125**, 034502.

Cornell, W.D., Cieplak, P., Bayly, C.I., Gould, I.R., Merz, K.M., Ferguson, D.M., and Kollman, P.A. (1995) A second generation force field for the simulation of proteins, nucleic acids, and organic molecules. *Journal of the American Chemical Society*, **117**, 5179−5197.

Cygan, R.T., Liang, J.J., and Kalinichev, A.G. (2004) Molecular models of hydroxide, oxyhydroxide, and clay phases and the development of a general force field. *The Journal of Physical Chemistry B*, **108**, 1255−1266.

Cygan, R.T., Greathouse, J.A., Heinz, H., and Kalinichev, A.G. (2009) Molecular models and simulations of layered materials. *Journal of Materials Chemistry*, **19**, 2470−2481.

Dauber-Osguthorpe, P., Roberts, V.A., Osguthorpe, D.J., Wolff, J., Genest, M., and Hagler, A.T. (1988) Structure and energetics of ligand binding to proteins: Escherichia coli dihydrofolate reductase-trimethoprim, a drug-receptor system. *Proteins: Structure, Function, and Bioinformatics*, **4**, 31−47.

Dellinger, A.L., Cunin, P., Lee, D., Kung, A.L., Brooks, D.B., Zhou, Z., and Kepley, C.L. (2015) Inhibition of inflammatory arthritis using fullerene nanomaterials. *PloS One*, **10**, e0126290.

Evans, D.J. and Holian, B.L. (1985) The nose−hoover thermostat. *The Journal of Chemical Physics*, **83**, 4069−4074.

Fortner, J.D., Lyon, D.Y., Sayes, C.M., Boyd, A.M., Falkner, J.C., Hotze, E.M., and Colvin, V.L. (2005) C_{60} in water:

nanocrystal formation and microbial response. *Environmental Science & Technology*, **39**, 4307−4316.

Fortner, J.D., Solenthaler, C., Hughes, J.B., Puzrin, A.M., and Plotze, M. (2012) Interactions of clay minerals and a layered double hydroxide with water stable, nano scale fullerene aggregates (nc(60)). *Applied Clay Science*, **55**, 36−43.

Gogotsi, Y. (editor) (2006) *Nanomaterials Handbook*. CRC Press, Boca Raton, Florida, USA.

Goyal, R.N., Gupta, V.K., Sangal, A., and Bachheti, N. (2005) Voltammetric determination of uric acid at a fullerene-C_{60}-modified glassy carbon electrode. *Electroanalysis*, **17**, 2217−2223.

Greathouse, J.A. and Cygan, R.T. (2005) Molecular dynamics simulation of uranyl (VI) adsorption equilibria onto an external montmorillonite surface. *Physical Chemistry Chemical Physics*, **7**, 3580−3586.

Grim, R.E. (1968) *Clay Mineralogy*. McGraw-Hill Book Co., New York.

Gruner, J.W. (1934) The crystal structures of talc and pyrophyllite. *Zeitschrift fü Kristallographie − Crystalline Materials*, **88**, 412−419.

Guldi, D.M., Luo, C., Swartz, A., Gómez, R., Segura, J.L., Martín, N., and Sariciftci, N.S. (2002) Molecular engineering of C_{60}-based conjugated oligomer ensembles: Modulating the competition between photoinduced energy and electron transfer processes. *The Journal of Organic Chemistry*, **67**, 1141−1152.

Han, J., Zhuo, Y., Chai, Y.Q., Xiang, Y., and Yuan, R. (2015) New type of redox nanoprobe: C_{60}-based nanomaterial and its application in electrochemical immunoassay for doping detection. *Analytical Chemistry*, **87**, 1669−1675.

Heinz, H. (2012) Clay minerals for nanocomposites and biotechnology: surface modification, dynamics and responses to stimuli. *Clay Minerals*, **47**, 205−230.

Heinz, H., Koerner, H., Anderson, K.L., Vaia, R.A., and Farmer, B.L. (2005) Force field for mica-type silicates and dynamics of octadecylammonium chains grafted to montmorillonite. *Chemistry of Materials*, **17**, 5658−5669.

Hendricks, S.B. (1940) Variable structures and continuous scattering of X-rays from layer silicate lattices. *Physical Review*, **57**, 448−454.

Hess, B., Bekker, H., Berendsen, H.J., and Fraaije, J.G. (1997) LINCS: a linear constraint solver for molecular simulations. *Journal of Computational Chemistry*, **18**, 1463−1472.

Hess, B., Kutzner, C., Van Der Spoel, D., and Lindahl, E. (2008) GROMACS 4: algorithms for highly efficient, load-balanced, and scalable molecular simulation. *Journal of Chemical Theory and Computation*, **4**, 435−447.

Hou, W.C., Moghadam, B.Y., Westerhoff, P., and Posner, J.D. (2011) Distribution of fullerene nanomaterials between water and model biological membranes. *Langmuir*, **27**, 11899−11905.

Jafvert, C.T. and Kulkarni, P.P. (2008) Buckminsterfullerene's (C_{60}) octanol−water partition coefficient (K ow) and aqueous solubility. *Environmental Science & Technology*, **42**, 5945−5950.

Jorgensen, W.L., Maxwell, D.S., and Tirado-Rives, J. (1996) Development and testing of the OPLS all-atom force field on conformational energetics and properties of organic liquids. *Journal of American Chemical Society*, **118**, 11225−11236.

Kim, H., Bedrov, D., and Smith, G.D. (2008) Molecular dynamics simulation study of the influence of cluster geometry on formation of C_{60} fullerene clusters in aqueous solution. *Journal of Chemical Theory and Computation*, **4**, 335−340.

Kouijzer, S., Li, W., Wienk, M.M., and Janssen, R.A.J. (2014) Charge transfer state energy in ternary bulk-heterojunction polymer−fullerene solar cells. *Journal of Photonics for Energy*, **5**, 057203−057203.

Labille, J., Masion, A., Ziarelli, F., Rose, J., Brant, J., Villiéras, F., and Bottero, J.Y. (2009) Hydration and dispersion of C_{60} in aqueous systems: the nature of water−fullerene interactions. *Langmuir*, **25**, 11232−11235.

Lee, J.H. and Guggenheim, S. (1981) Single crystal X-ray refinement of pyrophyllite-1Tc. *American Mineralogist*, **66**, 350−357.

Li, L., Bedrov, D., and Smith, G.D. (2005) A molecular-dynamics simulation study of solvent-induced repulsion between C_{60} fullerenes in water. *The Journal of Chemical Physics*, **123**, 204504.

Li, Q., Xie, B., Hwang, Y.S., and Xu, Y. (2009) Kinetics of C_{60} fullerene dispersion in water enhanced by natural organic matter and sunlight. *Environmental Science & Technology*, **43**, 3574−3579.

Liu, D., Zhang, H., Zhang, Y., Liu, M., Wu, J., Pan, Y., and Zeng, Q. (2010) Effect of graphite carbon nanoparticles on cell growth in vitro. *Journal of Clinical Rehabilitative Tissue Engineering Research*, **14**, 443−446.

Liu, Y. (2009) Is the free energy change of adsorption correctly calculated? *Journal of Chemical and Engineering Data*, **54**, 1981−1985.

López-Lilao, A., Gómez-Tena, M.P., Mallol, G., and Monfort, E. (2017) Clay hydration mechanisms and their effect on dustiness. *Applied Clay Science*, **144**, 157−164.

Maciel, C., Fileti, E.E., and Rivelino, R. (2009) Note on the free energy of transfer of fullerene C_{60} simulated by using classical potentials. *The Journal of Physical Chemistry B*, **113**, 7045−7048.

Makov, G. and Payne, M.C. (1995) Periodic boundary conditions in ab initio calculations. *Physical Review B*, **51**, 4014.

Mauter, M.S. and Elimelech, M. (2008) Environmental applications of carbon-based nanomaterials. *Environmental Science & Technology*, **42**, 5843−5859.

Mayo, S.L., Olafson, B.D., and Goddard, W.A. (1990) DREIDING: a generic force field for molecular simulations. *Journal of Physical Chemistry*, **94**, 8897−8909.

Monticelli, L. (2012) On atomistic and coarse-grained models for C_{60} fullerene. *Journal of Chemical Theory and Computation*, **8**, 1370−1378.

Nosé, S. and Klein, M.L. (1983) Constant pressure molecular dynamics for molecular systems. *Molecular Physics*, **50**, 1055−1076.

Parrinello, M. and Rahman, A. (1981) Polymorphic transitions in single crystals: A new molecular dynamics method. *Journal of Applied Physics*, **52**, 7182−7190.

Pumera, M. (2010) Graphene-based nanomaterials and their electrochemistry. *Chemical Society Reviews*, **39**, 4146−4157.

Qiao, R., Roberts, A.P., Mount, A.S., Klaine, S.J., and Ke, P.C. (2007) Translocation of C_{60} and its derivatives across a lipid bilayer. *Nano Letters*, **7**, 614−619.

Robinson, G.W., Singh, S., Zhu, S.B., and Evans, M.W. (1996) *Water in Biology, Chemistry and Physics: Experimental Overviews and Computational Methodologies* (Vol. 9). World Scientific Publications, London.

Ryckaert, J.P., Ciccotti, G., and Berendsen, H.J. (1977) Numerical integration of the cartesian equations of motion of a system with constraints: molecular dynamics of n-alkanes. *Journal of Computational Physics*, **23**, 327−341.

Sayes, C.M., Fortner, J.D., Guo, W., Lyon, D., Boyd, A.M., Ausman, K.D., and West, J.L. (2004) The differential cytotoxicity of water-soluble fullerenes. *Nano Letters*, **4**, 1881−1887.

Scida, K., Stege, P.W., Haby, G., Messina, G.A., and García, C.D. (2011) Recent applications of carbon-based nanomaterials in analytical chemistry: critical review. *Analytica*

Chimica Acta, **691**, 6−17.

Song, M., Yuan, S., Yin, J., Wang, X., Meng, Z., Wang, H., and Jiang, G. (2012) Size-dependent toxicity of nano-C$_{60}$ aggregates: more sensitive indication by apoptosis-related Bax translocation in cultured human cells. *Environmental Science & Technology*, **46**, 3457−3464.

Teppen, B.J., Yu, C.H., Miller, D.M., and Schäfer, L. (1998) Molecular dynamics simulations of sorption of organic compounds at the clay mineral/aqueous solution interface. *Journal of Computational Chemistry*, **19**, 144−153.

Thundat, T., Warmack, R.J., Ding, D., and Compton, R.N. (1993) Atomic force microscope investigation of C$_{60}$ adsorbed on silicon and mica. *Applied Physics Letters*, **63**, 891−893.

Tremblay, J.F. (2002) Mitsubishi chemical aims at breakthrough. *Chemical & Engineering News*, **80**, 16−17.

Vasconcelos, I.F., Bunker, B.A., and Cygan, R.T. (2007) Molecular dynamics modeling of ion adsorption to the basal surfaces of kaolinite. *The Journal of Physical Chemistry C*, **111**, 6753−6762.

Warne, M.R., Allan, N.L., and Cosgrove, T. (2000) Computer simulation of water molecules at kaolinite and silica surfaces. *Physical Chemistry Chemical Physics*, **2**, 3663−3668.

Yu, C.H., Newton, S.Q., Norman, M.A., Miller, D.M., Schäfer, L., and Teppen, B.J. (2000a) Molecular dynamics simulations of the adsorption of methylene blue at clay mineral surfaces. *Clays and Clay Minerals*, **48**, 665−681.

Yu, C.H., Norman, M.A., Newton, S.Q., Miller, D.M., Teppen, B.J., and Schäfer, L. (2000b) Molecular dynamics simulations of the adsorption of proteins on clay mineral surfaces. *Journal of Molecular Structure*, **556**, 95−103.

Zhang J., Li, D., Li, Y., Wang, C., He, N., Liu, Y., and Zhang, J. (2011) Oxidative damages of fullerenes on human embryo liver cells. *Asian Journal of Ecotoxicology*, **6**, 149−153.

Zhu, R., Chen, W., Shapley, T.V., Molinari, M., Ge, F., and Parker, S.C. (2011) Sorptive characteristics of organomontmorillonite toward organic compounds: a combined LFERs and molecular dynamics simulation study. *Environmental Science & Technology*, **45**, 6504−6510.

Zhu, R., Molinari, M., Shapley, T.V., and Parker, S.C. (2013) Modeling the interaction of nanoparticles with mineral surfaces: Adsorbed C$_{60}$ on pyrophyllite. *Journal of Physical Chemistry A*, **117**, 6602−6611.